

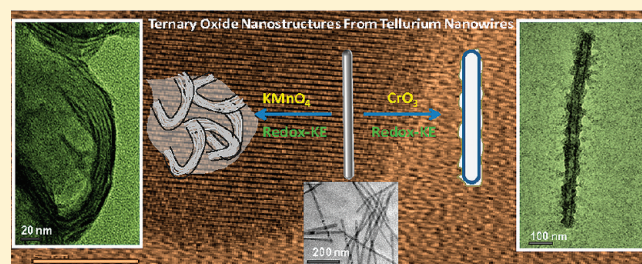
Tubular Nanostructures of $\text{Cr}_2\text{Te}_4\text{O}_{11}$ and Mn_2TeO_6 through Room-Temperature Chemical Transformations of Tellurium Nanowires

T. S. Sreepasad and T. Pradeep*

DST Unit of Nanoscience, Department of Chemistry, Indian Institute of Technology Madras, Chennai-600 036, India

Supporting Information

ABSTRACT: Tubular ternary nanostructures of tellurium were made through chemical transformations of tellurium nanowires (Te NWs). These transformations occur through reactions with CrO_3 and KMnO_4 , two of the strongest oxidizing agents. In the case of CrO_3 , the 1D structure of the NWs remained intact and the morphology changed to hollow wires of $\text{Cr}_2\text{Te}_4\text{O}_{11}$, but reaction with KMnO_4 resulted in the loss of 1D structure, forming a carbon onion-like object composed of Mn_2TeO_6 . As the reaction proceeded, the crystallinity of the NWs decreased, and the final products were amorphous. The reaction products were characterized using different spectroscopic and microscopic techniques. Time-dependent transmission electron microscopic (TEM) analysis of both of the reaction products showed that first a shell is formed around the NWs. Further reaction results in the formation of hollow structures. During the reaction with CrO_3 , TEM in the intermediate stages showed that the periphery of the material was amorphous, whereas the inside, where unreacted parts of Te NWs remained, was crystalline with a clear lattice structure. X-ray photoelectron spectroscopy (XPS) as well as Raman spectroscopy showed a redox reaction in both cases. Studies suggest that both redox reactions and nanoscale Kirkendall effect might be involved in the formation mechanism.



INTRODUCTION

Hollow nanostructures have attracted a great deal of attention because of the unique physical and chemical properties they exhibit. The high surface areas and low material density make them ideal candidates for potential applications such as high-efficiency catalysts or drug-delivery agents.¹ Hollow 1D nanostructures with tubular morphology have attracted growing interest. Tubular nanostructures made of semiconductors,² metals,^{3,4} ferroelectrics,⁵ and magnetic⁶ materials have all been studied extensively. Various strategies such as rolling up of layered materials or via an axial growth in a rolled-up form,⁷ etching the core of a core-shell nanowire,⁸ and creating pores in templates⁹ have been employed to synthesize tubular structures.

Metal oxide nanostructures, especially ternary metal oxide nanostructures, are of deep scientific interest because of their structure-dependent optical, electronic, mechanical, and catalytic properties.^{10–16} They have a broad range of technological applications such as transistors and computing devices. Direct large scale synthesis of these materials, in an environmental friendly manner, with control over nanoparticle structure, surface chemistry, monodispersity, crystal structure, and assembly has been a long-standing problem.¹⁰ Compared with anisotropic structures made of other materials, ternary oxide structures are very few, and because of the dearth of material availability, the mechanical, transport, photoconductive, thermoelectric, electronic, optical, and catalytic properties of such materials are mostly

studied theoretically.¹⁰ Hence, there is an interest to devise synthetic strategies to generate technologically relevant anisotropic ternary oxide structures.

An alternate for the direct synthesis is to devise strategies to manipulate postsynthetically already formed structures by chemical treatments to fine-tune size, shape, or composition. Postsynthetic manipulation of nanostructures,^{17–20} especially the anisotropic ones,^{19,21,22} has attracted growing interest because it allows compositional modifications or even yields novel structures with multiple components. Such variations may not be possible through direct synthetic processes. Through precise control over reaction conditions, unconventional shapes with versatile crystal structures can be created because of the high mechanical stress generated during some transformations.²³ Te nanowires (Te NWs) are versatile nanosystems, having a large number of application possibilities.²⁴ The reduction potential of the $\text{TeO}_3^{2-}/\text{Te}$ system (0.589 V)²⁵ allows the possibility of galvanic-type reactions also. Reactions of Te NWs resulting in the formation of metallic composites are well-documented.^{26,27} Utilizing the reduction ability of Te NWs, novel leaf-like graphenic structures have been created.²⁸ Te NWs have been used as sacrificial templates for the synthesis of various 1D nanostructures of Pt

Received: May 10, 2011

Revised: July 19, 2011

Published: July 19, 2011

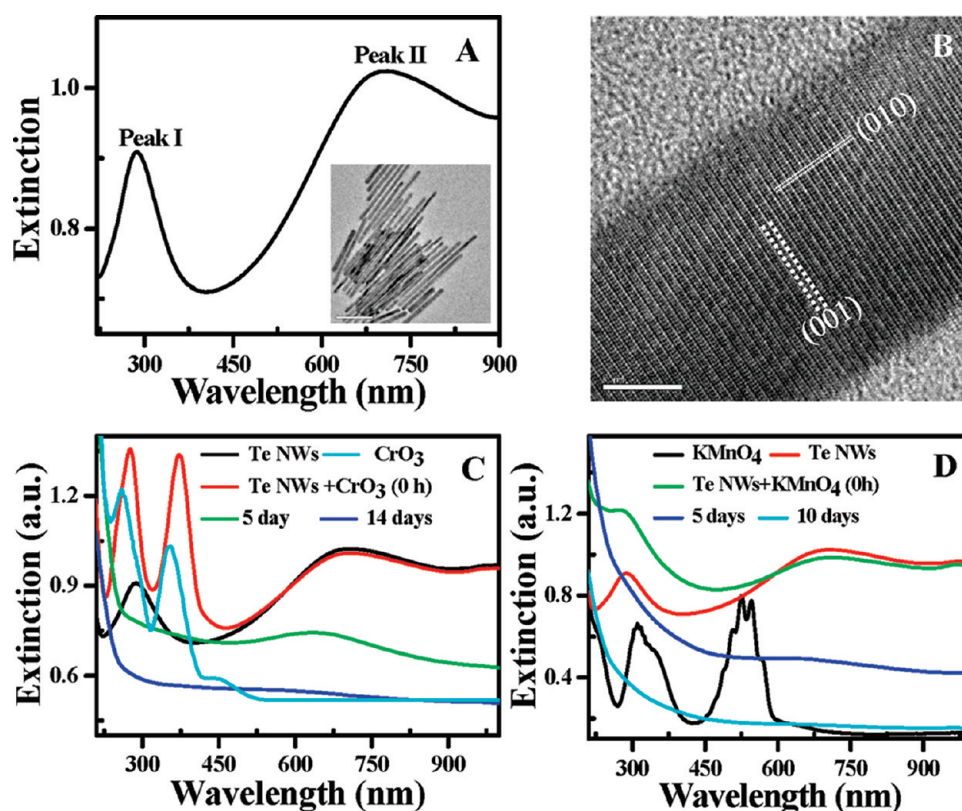


Figure 1. (A) UV/vis spectrum of Te NWs. Peaks I and II indicated in the spectrum. Inset shows the large area TEM image of the Te NWs. Scale bar is 200 nm. (B) Lattice resolved image of an NW. Scale bar is 5 nm. Representative planes are marked. Representative time-dependent UV/vis spectra of reaction of Te NWs with 1 mM (C) CrO_3 and (D) KMnO_4 .

and Pd as well.²⁶ Reactivity of Te NWs with thiol-containing molecules was probed recently.²⁹ Postsynthetic reactions of Te NWs are known to improve the surface-enhanced Raman scattering (SERS) properties.^{30,31} Still, compared with other 1D nanostructures like gold nanorods, tuning the useful properties of Te NWs postsynthetically via different reactions remains a rather poorly investigated field.

In this Article, through a postsynthetic chemical route, a facile way to fabricate tellurium-based nanoscale ternary oxide structures is presented. No report for the direct synthesis of such structures exists in the literature. A novel shape transformation of Te NWs induced by $\text{CrO}_3/\text{KMnO}_4$ is utilized for the generation of ternary hollow structures. Reaction with CrO_3 resulted in the formation of hollow wires composed of $\text{Cr}_2\text{Te}_4\text{O}_{11}$. Carbon onion-like structures made up of Mn_2TeO_6 were formed when Te NWs were treated with KMnO_4 . The reactions were followed time-dependently using various spectroscopic and microscopic techniques, and a mechanism has been proposed. The present data suggest the involvement of redox reaction and nanoscale Kirkendall effect (NKE) during the transformations. Coupling these two effects might be a new step forward in tuning the size or shape as well as composition in one step.

MATERIALS AND METHODS

Sodium dodecyl sulfate (SDS, $\text{C}_{12}\text{H}_{25}\text{O}_4\text{SNa}$, 99%) was obtained from Acros. Tellurium dioxide powder (TeO_2 , 99.9%) was purchased from Alfa Aesar. Hydrazine monohydrate ($\text{N}_2\text{H}_4 \cdot \text{H}_2\text{O}$, 99–100%) and chromium trioxide (CrO_3) were purchased from SD Fine chemicals. Potassium permanganate (KMnO_4) was

purchased from Merck. All chemicals were used as received without any additional purification. Triply distilled water was used all through this study.

Synthesis of Te Nanowires (Te NWs). Te NWs were synthesized according to a reported procedure.³² TeO_2 powder was reduced using hydrazine hydrate in a beaker under constant stirring. After 1 h, the color of the solution changed from colorless to blue, indicating the formation of Te NWs. The reaction was arrested by the addition of SDS, which also protects the Te NWs formed. The as-prepared dispersion was centrifuged at 10 000 rpm for 15 min to remove excess reactants. The centrifugation was repeated two more times, and the residue was redispersed in distilled water so that the optical density at peak II is ~ 1 .

Reaction with $\text{CrO}_3/\text{KMnO}_4$. To 5 mL of Te NWs, 50 μL of 100 mM $\text{CrO}_3/\text{KMnO}_4$ was added. It was stirred for 5 min. The mixture was kept undisturbed under ambient conditions, and the reaction was monitored time-dependently using various spectroscopic and microscopic techniques.

Instrumentation. UV/vis spectrum of each sample was measured time-dependently using a Perkin-Elmer Lambda 25 UV/vis spectrophotometer. Small aliquots of the reaction mixture were dropped onto a carbon-coated copper grid at specific reaction time and dried under the ambient conditions. These samples were examined using a JEOL 3011, 300 kV high-resolution transmission electron microscope (HRTEM) with a UHR pole piece. Detailed control experiments involving UV/vis and HRTEM were performed. Raman spectra were measured with a WiTec GmbH confocal micro Raman spectrometer, typically with an excitation of 532 nm. XPS measurements were

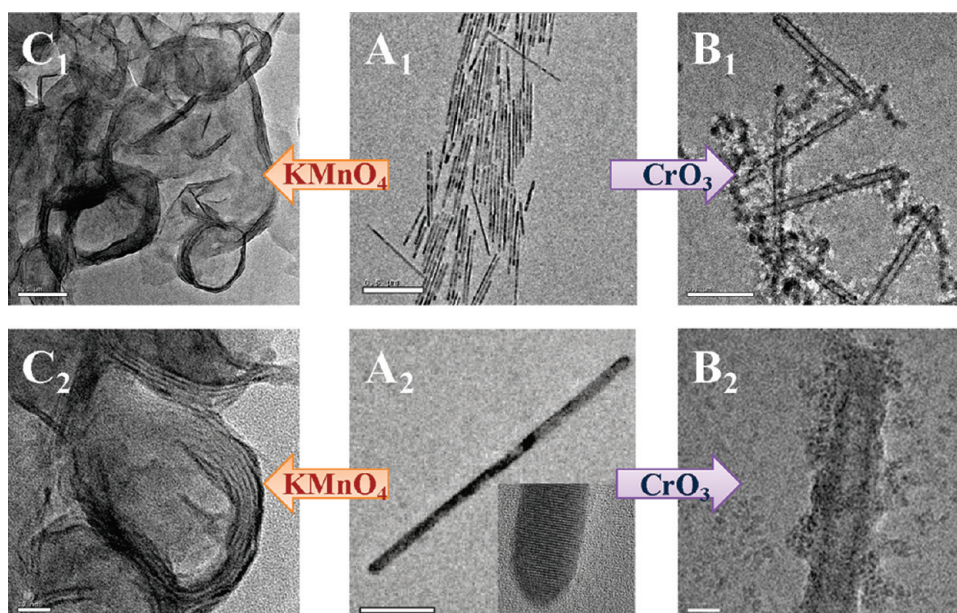


Figure 2. TEM images of starting Te NWs (A_1 and A_2) and the final reaction product with CrO_3 (B_1 and B_2 , after 14 days) and KMnO_4 (C_1 and C_2 , after 10 days). Scale bars in nanometers are A_1 (500), A_2 (100), B_1 (200), B_2 (20), C_1 (100), and C_2 (20). Inset in A_2 shows a higher magnification lattice resolved image of the tip of a starting NW. Scale bar corresponds to 5 nm.

done with Omicron ESCAProbe spectrometer with unmonochromatized Mg $K\alpha$ X-rays ($h\nu = 1253.6$ eV). Six spectra in the desired binding energy range were averaged. The samples were spotted as dropcast films on the sample stub and dried. The energy resolution of the spectrometer was set at 0.1 eV at a pass energy of 20 eV for typical measurements.

RESULTS AND DISCUSSION

Figure 1A shows the UV/vis spectrum of the as-prepared Te NWs after two rounds of centrifugation–redispersion cycles. Two prominent characteristic features can be seen in the spectrum. Peak I featuring around 280–300 nm corresponds to the transition from p-bonding valence band (VB_2) to the p-antibonding conduction band (CB_1). Peak II due to the transition from the p-lone pair valence band (VB_3) to the p-antibonding conduction band (CB_1) comes around 650–750 nm and is reported to shift to a higher wavelength region as the length of the NWs increases.^{28,32} For a particular synthesis, peak I was found to be at 288 nm and peak II was at 704 nm. The inset in Figure 1A shows the large area TEM images of the sample. The NWs are well-dispersed without any aggregation. The diameter was found to be 20 ± 2 nm. Figure 1B shows the lattice-resolved TEM image of the body of a Te NW. We can see that the NWs to begin with are highly crystalline, devoid of any defects or dislocations. The two representative planes of t-Te NWs, with interplanar spacings of 0.59 and 0.39 nm corresponding to $\{001\}$ and $\{010\}$, respectively, are marked in the Figure by dotted lines.^{29,32} We see that the NWs are highly anisotropic with perfect 1D structure.

Reaction between Te NWs and $\text{CrO}_3/\text{KMnO}_4$. Upon reaction with CrO_3 or KMnO_4 , UV/vis spectrum of the NWs undergoes marked changes. Figure 1C shows the representative time-dependent UV/vis spectrum of reaction between Te NWs and CrO_3 (1 mM). Complete time-dependent data is given in the Supporting Information (Supporting Information, Figure S1A). After mixing Te NWs with CrO_3 , peak II remained unchanged;

however, peak I was masked by the absorbance due to CrO_3 .³³ In presence of Te NWs, the CrO_3 peak was slightly red-shifted. After 1 day, the intensity of these peaks decreased, implying the reduction of CrO_3 (Supporting Information, Figure S1A). Peak II showed a slight decrease in intensity. The position was slightly blue-shifted as well. As reaction time progressed, the decrease in intensity as well as the blue-shift of peak II continued. The blue-shift of peak II indicates reaction of NWs and possibly a decrease in length. Subsequently, peak I begins to vanish. After 5 days, peak I was flattened completely, and no feature was found around 300 nm. After 14 days, both peaks I and II were almost absent. After this, no further change was observed. The blue color of the solution became transparent in this stage.

The reaction with KMnO_4 also showed substantial spectral changes (Figure 1D). Detailed time-dependent spectral changes are given in the Supporting Information (Figure S1B). Here, immediately after mixing of KMnO_4 , Te NW features showed changes. No spectral feature corresponding to KMnO_4 was visible in the spectrum. Peak I increased in intensity and was flattened slightly. Peak II decreased in intensity and showed a blue shift. After 1 day, peak I almost vanished completely, and peak II showed a blue shift accompanied by a gradual decrease in intensity (Supporting Information, Figure S1B). With progress in time, peak I completely disappeared, and peak II continued to decrease in intensity with the concurrent blue shift. After 10 days, the UV/vis spectrum did not show any characteristic features. As in the case of CrO_3 , the color of the solution after 10 days changed from blue to colorless. No further change was observed in the UV/vis spectrum, pointing to the completion of reaction.

The products of the reactions at various stages were characterized using TEM extensively. Figure 2 shows the TEM images of starting Te NWs and the reaction products (after 14 days of reaction) with CrO_3 and KMnO_4 (after 10 days of reaction). In the case of CrO_3 , the reaction results in hollow wires. In this case, the initial 1D structure of the precursor remained the same. Starting Te NWs were crystalline without

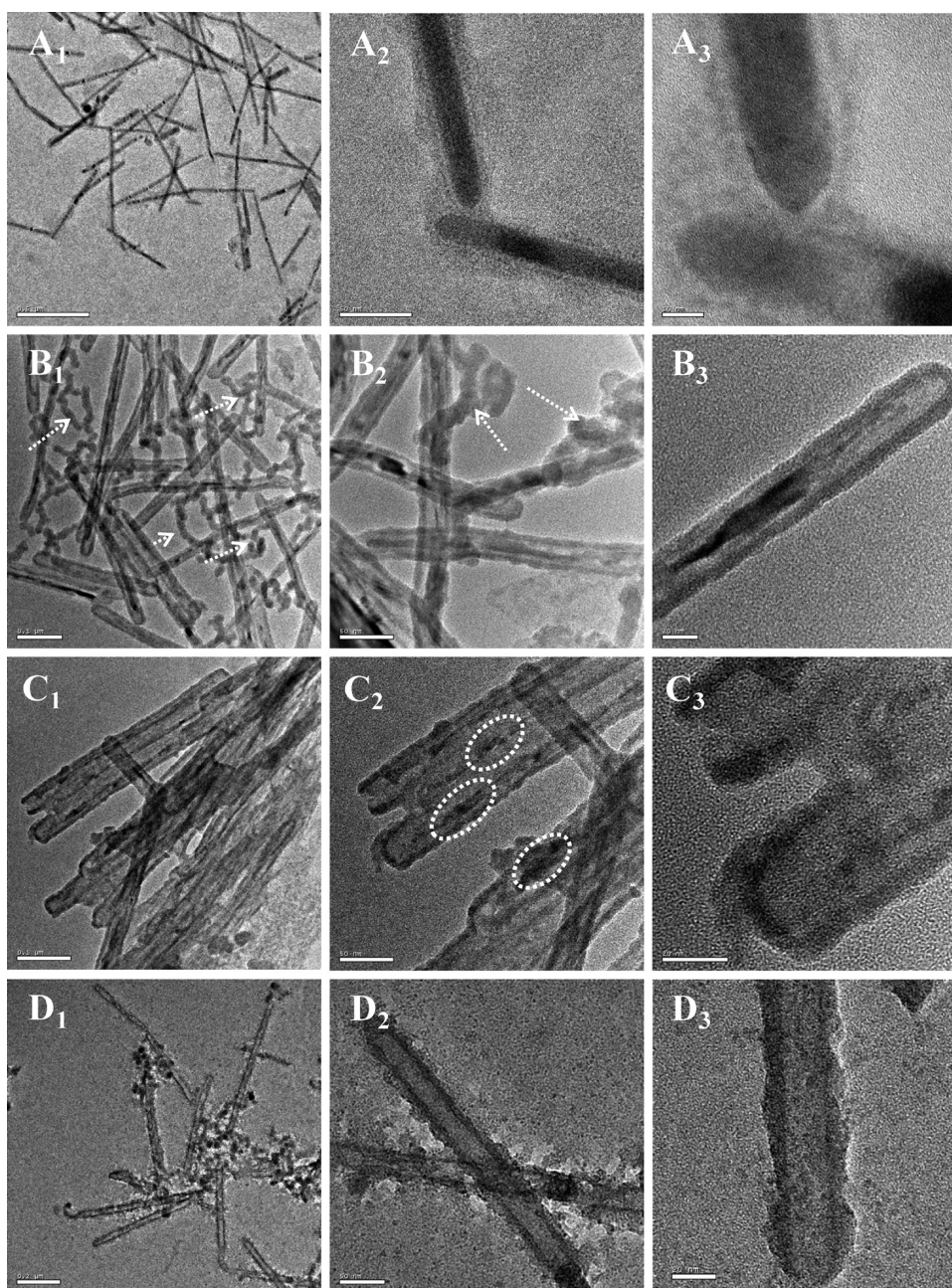


Figure 3. Time-dependent TEM images of the reaction between Te NWs and CrO_3 . From top to bottom, A_1 to D_1 , the time of reaction increases. For each of the four samples, the expanded views are on the right. (A_1 – A_3) 1 day, (B_1 – B_3) 5 days, (C_1 – C_3) 10 days, and (D_1 – D_3) 14 days. In C_2 , traces of initial NWs are marked with white circles. Worm-like structures formed after 5 days are marked by white arrows in B_1 and B_2 . Scale bars in nm are: A_1 (500), B_1 and C_1 (100), D_1 (200), A_2 – D_2 (50), A_3 (10), and B_3 – D_3 (20).

any defects (Figure 2 A_2). Inset shows the lattice-resolved image of a tip of the parent NW, which confirms the single crystalline structure. In contrast, after treatment with CrO_3 , structures with hollow interiors have formed (Figure 2 B_1 , B_2). The exterior of the wires showed a crusty structure with small nanoparticles embedded on it. However, in the case of KMnO_4 , the 1D structure of the NWs was disrupted. Figure 2 C_1 , C_2 shows TEM images of the final product having a scaly structure with concentric ring-like ridges similar to the carbon onions (Figure 2 C_2), although the present structures are 2D, unlike in the case of the onions, which are 3D. The edge of the film was thicker, and the structure resembled the walls of multiwalled carbon nanotubes (MWNTs).

In the next few Figures, we discuss the reactions of CrO_3 and KMnO_4 separately. Shape transformations of Te NWs were followed time-dependently using TEM, and the intermediate structures were analyzed to get insight into the reaction mechanism. Figure 3 shows the TEM images of NWs at various stages of the reaction with CrO_3 (1 mM). After 1 day (Figure 3 A_1 – A_3), a thin layer was formed around the surface of Te NWs forming core–shell like structures. Te NWs are known to reduce metal ions.^{25–27} The reduction potential of Te/Cr couple enables the reduction of Cr(VI) and oxidation of Te(0). Hence, the surface atoms of Te NWs might be reducing the CrO_3 present in the solution, which is deposited over the NWs. This gives rise

to the core–shell structure observed in TEM and creates an interface as well. UV/vis spectral changes indicate the reduction of CrO_3 during this time interval, emphasizing the above proposition. So, the thin layer formed around Te NWs might be the reduction product of CrO_3 . As time progressed, the thickness of this layer increased (Figure 3B₁). Te NWs inside the side walls were reacted concurrently, forming voids within (Figure 3B₂). The reaction appears to start from the tip of the NWs (Figure 3B₃). The pits formed increased in size as time progressed. The length of the NWs formed within the shell

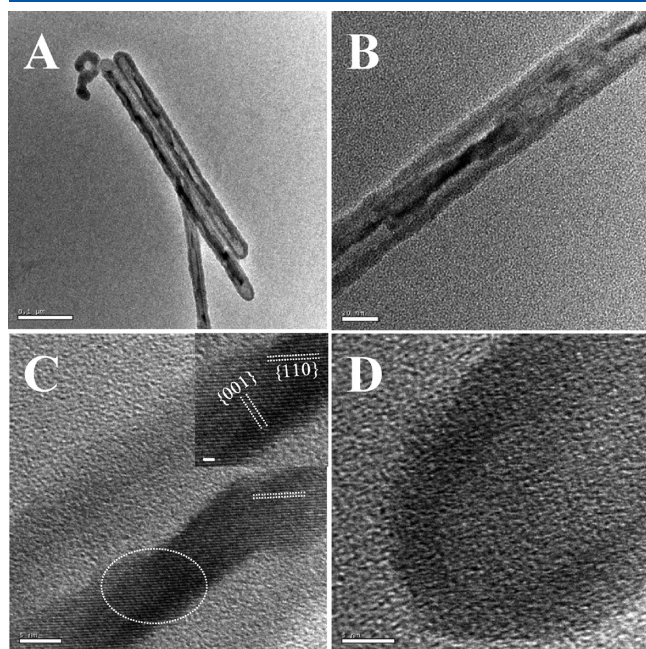


Figure 4. (A–D) TEM images of the sample after 5 days of reaction between Te NWs and CrO_3 . Scale bar in A is 100 nm, B is 20 nm, and C and D are 5 nm, respectively. Inset in C shows the higher magnification image of the part marked in C. Inset scale bar is 2 nm.

decreased with time (Figure 3B₂,B₃). This is consistent with the blue shift of peak II in the UV/vis spectra.

Some worm-like structures were also seen as the reaction product at this phase of the reaction (marked by white dotted arrows in Figure 3B₁,B₂). After 10 days of reaction, the voids increased in dimension and resulted in the formation of hollow NWs. The structure almost completely transformed into hollow wires after 10 days (Figure 3C₁–C₃). Some traces of initial NWs were still seen in the structure (Figure 3C₂, marked by white dotted circles). In some cases, the tip of NWs opened, forming tubes (Figure 3C₃). After 14 days of reaction, the structures became completely hollow (Figure 3D₁–D₃). As previously discussed, the surface of the final structure was rough and many corrugations were seen (Figure 3D₂). The worm-like structures were observed less frequently as reaction time increased, and after 14 days of reaction, very few numbers of such structures were seen. The intermediate structures were selected and studied in detail to understand the crystal structure and composition. Figure 4A–D shows the TEM images of nanostructures formed after 5 days of reaction at different magnifications. The thick walls and the reacted parts of the Te NWs can be seen in Figure 4B. At higher magnification (Figure 4C), crystalline nature was seen only in the inner region of the structures (where reacted NWs were present). The image was slightly blurred because of the decrease in crystallinity. However, the higher magnification image (inset of Figure 4C) confirmed the presence of crystalline Te NWs. The lattice structure present was indexed as the {001} and {110} facets of t-Te. The periphery turned completely amorphous, showing no crystal planes. Figure 4D shows the high magnification image of the hollow tip of the formed structure. No lattice was seen, pointing to the loss of crystallinity during the reaction.

To understand the elemental composition of the product, we analyzed the intermediate structures using energy dispersive analysis of X-rays (EDAX). Figure 5 shows the TEM of the sample from where the EDAX spectrum and elemental maps were taken. The corresponding EDAX spectrum and elemental maps are also given. The elemental maps are rotated $\sim 45^\circ$ degrees counter-clockwise with respect to the TEM image. The

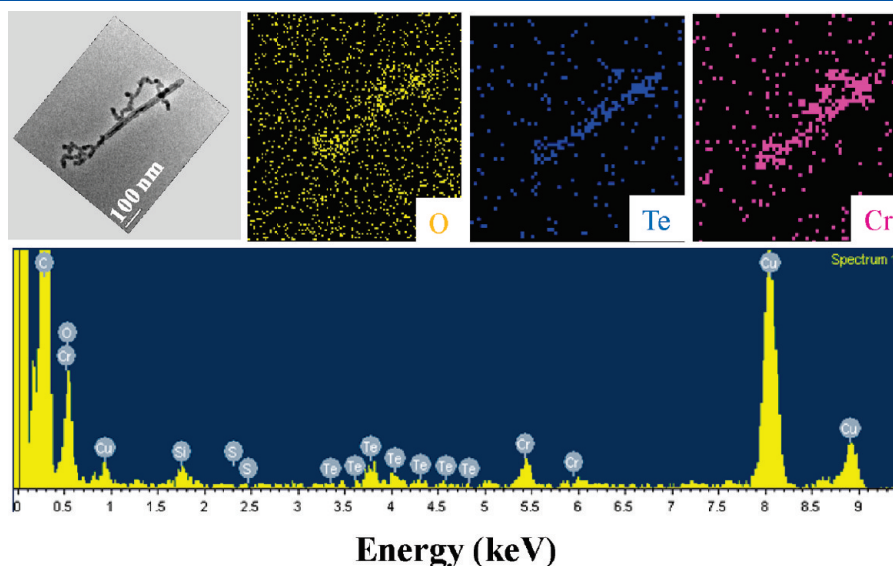


Figure 5. EDAX spectrum and elemental maps of the sample after 5 days of reaction pointing to the presence of tellurium, chromium, and oxygen in the structure. The carbon content in the EDAX spectrum is large in view of the carbon grid used. Cu is also due to the grid. TEM image is tilted $\sim 45^\circ$ to match the elemental images. Cu signatures in the EDAX spectrum are from the TEM grids.

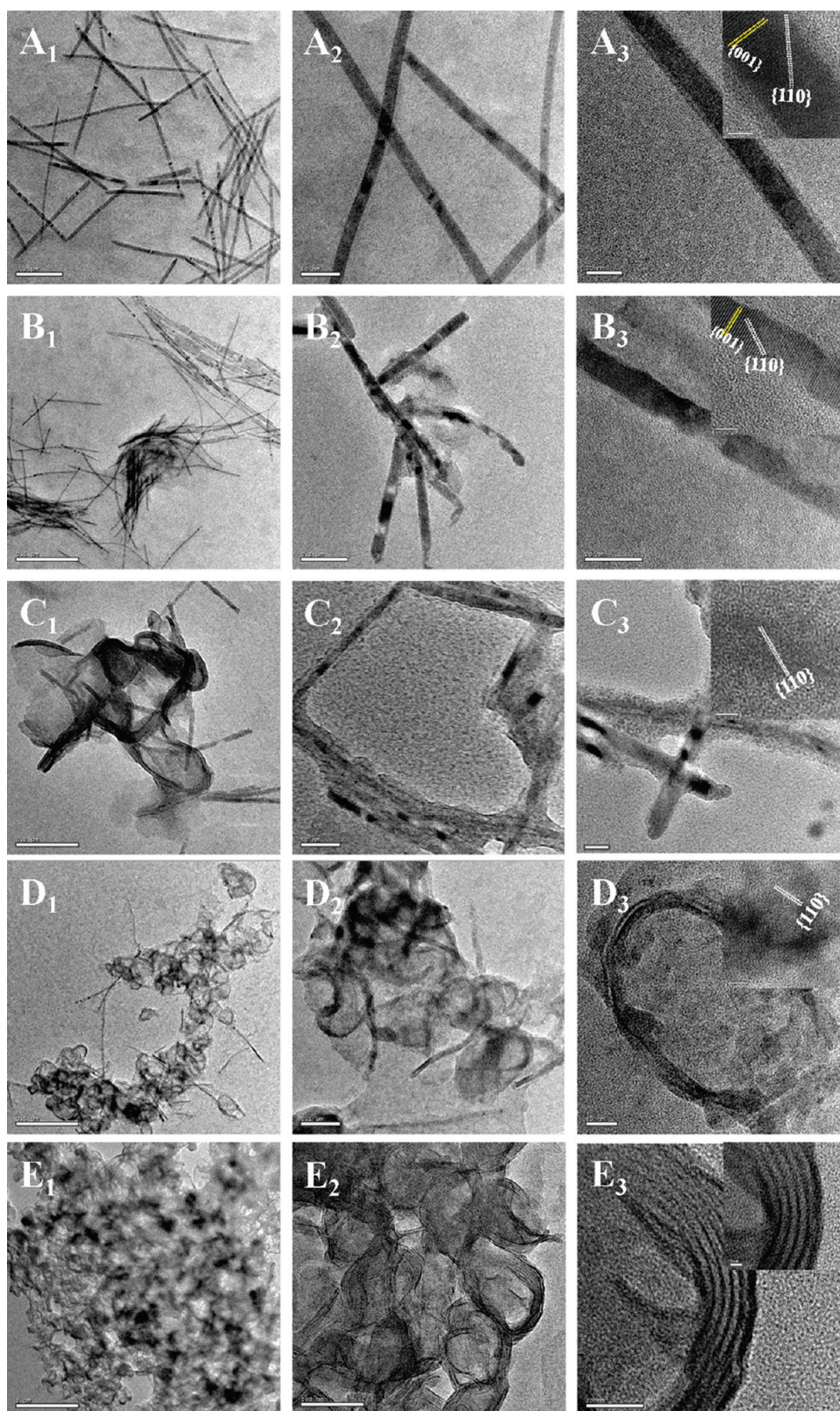


Figure 6. Time-dependent TEM images of Te NWs during the reaction with KMnO_4 . From top to bottom, the reaction time increases. For each set image, A_1 to E_1 , representing different days of reaction, the corresponding magnified images are on the right. TEM images were taken after (A_1 – A_3) 1 day, (B_1 – B_3) 3 days, (C_1 – C_3) 5 days, (D_1 – D_3) 8 days, and (E_1 – E_3) 10 days of reaction. Scale bars in A_1 and C_1 are 200 nm, B_1 and D_1 are 500 nm, E_1 is 1 μm , A_2 and C_2 are 50 nm, B_2 , D_2 , and E_2 are 100 nm, and A_3 – E_3 are 20 nm. Scale bars in the inset images are 5 nm.

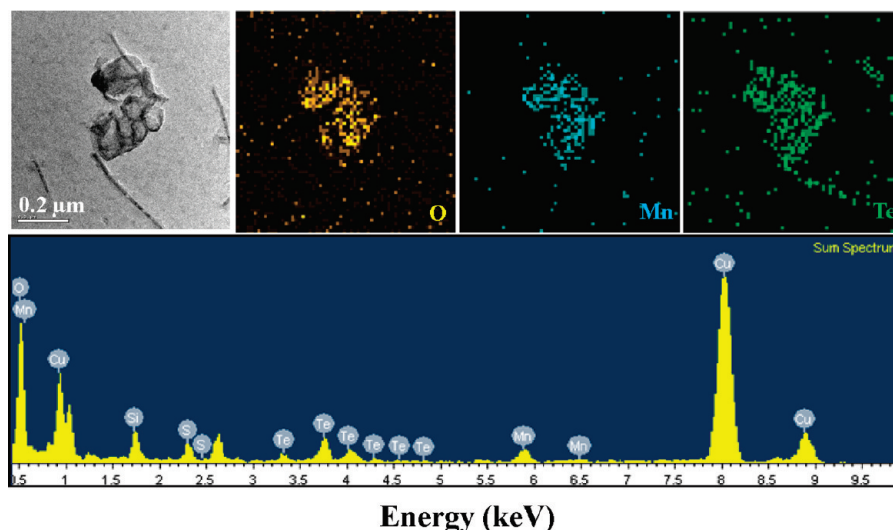


Figure 7. EDAX spectrum and elemental maps of the Te NW sample after 8 days of reaction with KMnO_4 confirming the presence of Te, Mn, and O in the final structure. The Cu features are originating from the underlying TEM grids.

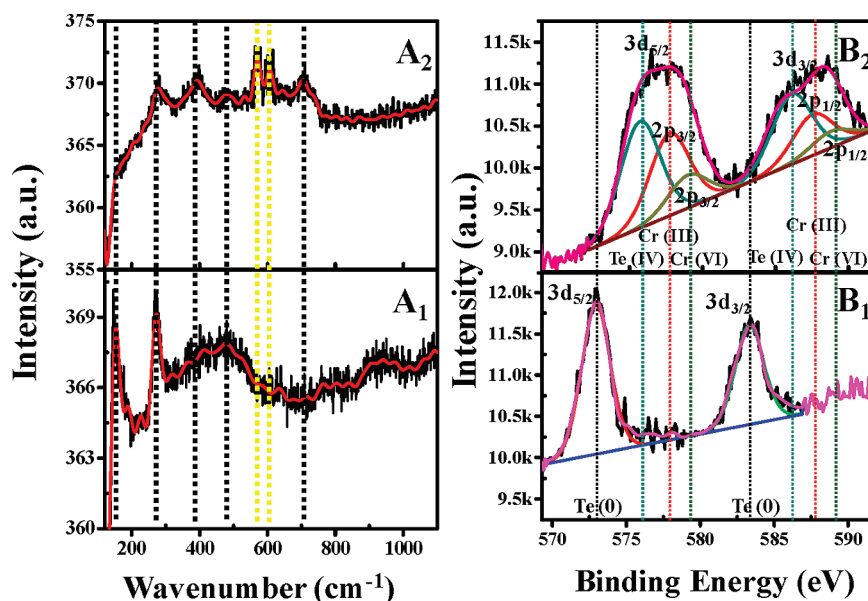


Figure 8. Raman spectrum of the Te NWs (A_1) before and (A_2) after reaction with CrO_3 . The peaks due to Te are marked with black dotted lines. The Cr(III) features are marked with yellow lines. XPS spectrum in the Te 3d region (B_1) before and (B_2) after the reaction of Te NWs with CrO_3 . The spectra have been decomposed to components. The component positions are marked by dotted lines.

sample represents Te NWs after 5 days of reaction with CrO_3 . It clearly shows the presence of Te, Cr, and O. We can see a 1:1 correspondence between the TEM image and the elemental maps. We conclude that the structure is primarily made up of Te, Cr, and O, pointing toward the formation of a ternary compound. Interestingly, the worm-like structures seen have higher Cr content. Similarly, all intermediate structures were analyzed using EDAX (Supporting Information, Figures S2–S4). All structures showed the presence of Te, Cr, and O, pointing to the suggestion that the hollow structures may be a ternary compound of Cr, Te, and O.

Similarly, reaction between Te NWs and KMnO_4 was also followed time-dependently by analyzing the intermediate products using TEM. Figure 6 shows the time-dependent changes of

Te NWs. After 1 day, a thin shell formed around the NWs, similar to the case of CrO_3 reaction (Figure 6A₁–A₃). As in the case of CrO_3 , the shell might be due to the reduction of KMnO_4 through a redox reaction between Te NWs and KMnO_4 , which is favorable when reduction potentials are considered. The formed shell was amorphous in nature, confirmed by the lattice image (inset of Figure 6A₃), which showed clear lattice in the inside core (Te NWs) and no lattice for the shell. Because of the decrease in crystallinity with reaction time, lattice-resolved images were not as clear as the initial NWs as the reaction time increased. After 3 days of reaction, the NWs bundled up with a thin film being formed around the bundles (Figure 6B₁). In some parts of the bundles, the NWs were seen with corrugated surfaces (Figure 6B₂). On closer examination, corrugations were found to

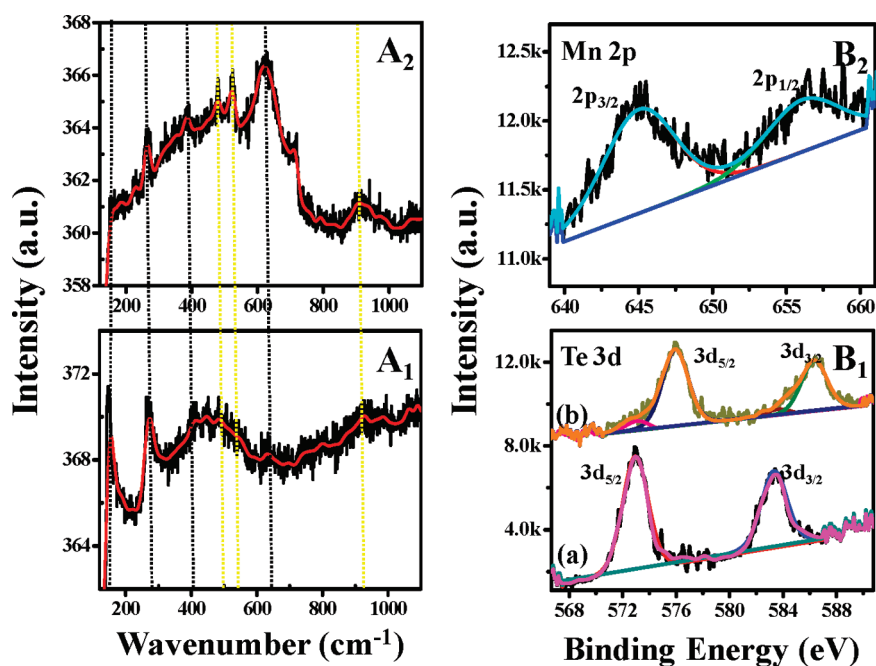
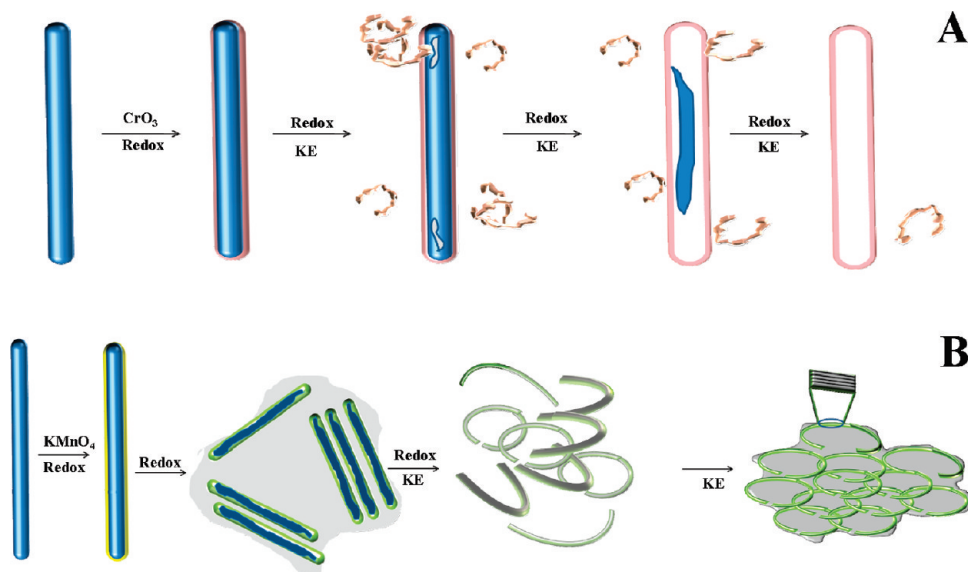


Figure 9. Raman spectrum of the Te NWs (A_1) before and (A_2) after the reaction with KMnO_4 . The peaks due to Te are marked with black dotted lines. The Mn(IV) features are marked with yellow dotted lines. XPS spectra in the (B_1) Te 3d region (a, before reaction; b, after reaction with KMnO_4) and (B_2) Mn 2p regions after the reaction of Te NWs with KMnO_4 .

Scheme 1. Schematic Representation of Different Stages of Reactions between Te NWs and (A) CrO_3 and (B) KMnO_4 .



be the pits formed due to the reaction (Figure 6B₃). The lattice-resolved image in the inset shows this aspect clearly. After 5 days of reaction, the shape was completely transformed into closed loop-like structures (Figure 6C₁). The formed structures had a thick wall and film-like interior. The thick walls resembled bent, reacted NWs. Some of the NWs came together and formed closed structures (Figure 6C₂). We can see that the NWs still have a shell around them. Nanowires showed reacted sidewalls with a corrugated structure. The sample was not as crystalline as the initial structure. The continuous lattice, which was seen in the initial NWs,

was not seen. Lattice structure was seen only at a few places. Figure 6C₃ shows a typical image of NWs after 5 days of reaction. We can see the {110} planes of Te in some parts (inset Figure 6C₃).

After 8 days of reaction, most of the NWs were converted to new structures (Figure 6D₁). Only a few NWs remained intact. It was evident from the Figure that the NWs are bending and forming the boundary of the formed structures (Figure 6D₂). Some reacted NWs can also be seen in the Figure. The crystallinity of the NWs decreased considerably by this time, and only very few places showed lattice structure (inset Figure 6D₃). The

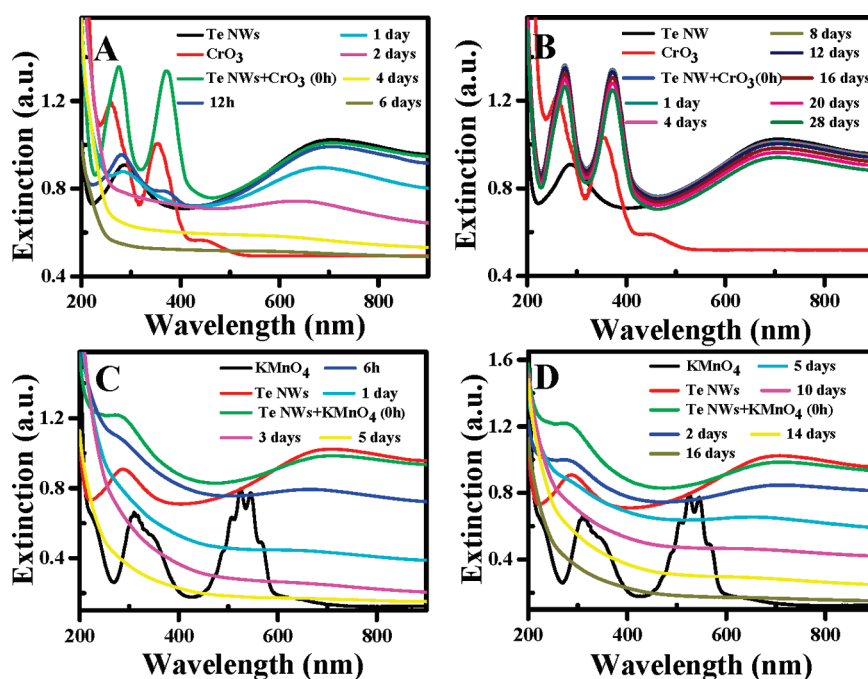


Figure 10. Effect of pH on the reaction between Te NWs and CrO₃ at pH (A) 3 and (B) 10. Effect of pH on the reaction between Te NWs and KMnO₄ at pH (C) 3 and (D) 10.

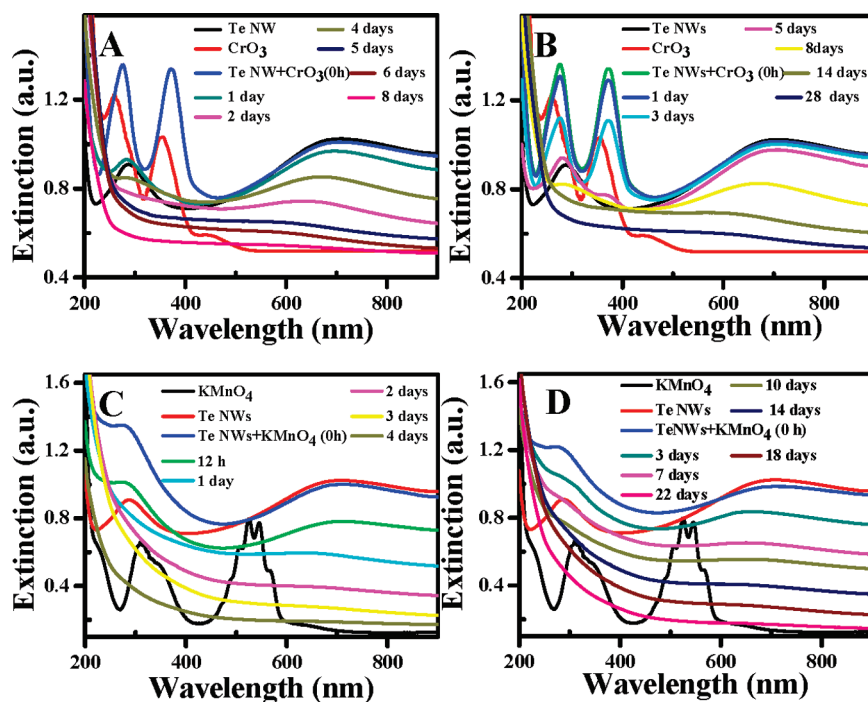


Figure 11. Effect of temperature on the reaction of Te NWs with CrO₃ at (A) 50 and (B) 10 °C. Effect of temperature on the reaction of Te NWs with KMnO₄ at (C) 50 and (D) 10 °C.

NWs started to become hollow as well (Figure 6D₃). After 10 days of reaction, no trace of NWs was seen, and only the new nanostructures remained. Figure 6E₁ shows the final structures formed after 10 days of reaction. No further change was observed to the structure. Side-walls or the boundary structure showed a remarkable change from the initial NWs. After 10 days of reaction, the sidewalls resembled walls of MWNTs. The

structure completely became amorphous, and no lattice imaging was possible in this stage.

All of these structures were analyzed using EDAX as well (Figure 7 and Supporting Information, Figure S5–S7). EDAX of structures after 3 days of reaction (where bundling up and film formation was seen) showed that they are mainly made up of Te, and the NWs remained more or less intact. Small amounts of O

and Mn were also present. This might be due to the thin shell formed due to the redox reaction. Amounts of Mn and O were prominent at the film-like regions (Supporting Information, Figure S5).

For longer reaction times, Mn and O signals were stronger (Supporting Information, Figures S6 and S7). Figure 7 shows the EDAX spectrum and elemental maps of structures formed after 8 days of reaction, where Te NWs almost completely changed to carbon onion-like structures. Te, Mn, and O were seen in the EDAX spectrum, indicating that the structure is a combination of these elements. The corresponding elemental maps confirmed this. Small parts of Te NWs that remained (seen in the TEM image in Figure 7) also can be seen in EDAX mapping. The product after 10 days of reaction was also analyzed by EDAX, which proved that the structures are mainly made up of Te, Mn, and O (Supporting Information, Figure S7). No trace of unreacted Te NWs was seen. Hence, it was concluded that the final structure is a ternary compound of Te, Mn, and O here as well.

EDAX measurements were useful in understanding the presence of various elements in the final reaction products, but the form in which the elements are present cannot be identified by EDAX. For this, the products of the reaction were analyzed using Raman and XPS. Figure 8A₁,A₂ shows the Raman spectra of the initial Te NWs and the product of the reaction with CrO₃, respectively. Te NWs are prone to undergo oxidation and hence have a thin layer of TeO₂ on the surface. Initial Te NWs showed three prominent features in the Raman spectrum at 149, 270, and 480 cm⁻¹ (marked with black lines). The feature at 149 cm⁻¹ is due to the tellurium oxide present on the surface.^{29–31,34} The feature at 270 nm is due to the second-order E mode of Te(0).²⁹ It can also have a contribution from Te–O vibration of the thin oxide layer or can also be due to the Te–S vibration.³⁴ The peak at 480 cm⁻¹ is due to the Te–O vibration of the oxide layer.^{29,30} The initial NWs had a broad feature in the 380–490 cm⁻¹ region, which might be a combination of two peaks centered at 392 and 480 cm⁻¹ due to the bending and symmetric stretching modes of Te–O.³⁴ After reaction with CrO₃, features due to the oxides of Te became more evident (Figure 8A₂). Te–O features at 270 and 481 cm⁻¹ were present in the sample, indicative of oxidation. In addition to this, new features at 392, 568, 610, and 710 cm⁻¹ became prominent after 14 days of reaction. Features at 392 and 710 cm⁻¹ are assigned to the bending and symmetric stretching modes of Te–O of TeO₂.³⁴ This points to the formation TeO₂ by the reaction between Te NWs and CrO₃. Two other features at 568 and 610 cm⁻¹ were seen and can be attributed to Cr₂O₃. (These are marked with yellow lines.) CrO₃ is known to show peaks at 220 and 360 cm⁻¹.³⁵ Cr(VI) is known to show a prominent feature at 845 cm⁻¹ (Cr–O–Cr vibrations of polychromate).³³ Absence of these features in the spectrum confirms the reduction. The spectral changes occurring after the reaction indicate a redox reaction between Te NWs and CrO₃, where Te(0) is oxidized to TeO₂ and Cr(VI) is reduced to Cr(III).

The sample was analyzed using XPS to find the oxidation state of the elements present. XPS scan in the 568–592 eV region is shown in Figure 8B. Parent NWs showed prominent features at 573.0 and 583.3 eV corresponding to Te 3d in the zerovalent state.³⁶ XPS trace after reaction with CrO₃ showed very broad features in the same region (Figure 8B₂). The spectrum has been decomposed to understand the components. Absence of feature at 573.0 eV indicates complete oxidation of Te(0).³⁶ Te showed 3d_{3/2} and 3d_{5/2} centered at 575.8 and 586.1 eV, respectively,

corresponding to Te(IV).³⁶ Besides Te 3d, Cr 2p also occurs in this region, and the spectrum is expectedly complex. The decomposed spectrum due to Te 3d shows a larger width than the starting NWs. Similarity in the binding energy of Te 3d and Cr 2p states may result in mixing of the final states, explaining the width. Similar increased width has been observed in the Te 3d region of ZnTe/Cr films, although the reason was not mentioned.³⁷ The presence of Cr in the Cr(III) oxidation state was also confirmed by XPS. Cr showed features at 577.8 and 587.6 eV corresponding to Cr 2p_{3/2} and 2p_{1/2} of Cr₂O₃.³⁶ The ΔJ value of 9.8 eV is in agreement with Cr(III).³⁸ Weaker features at 579.2 and 589.0 eV might be due to the residual CrO₃ present in the reaction mixture. Raman and XPS data confirmed a redox reaction between Te NWs and CrO₃. Among the possible ternary compounds of Te, Cr, and O, Cr₂Te₃O₉ and Cr₂Te₄O₁₁ were identified to be the likely candidates based on the oxidation potentials of Te and Cr.^{39,40} Because the Raman spectra indicated TeO₂ and Cr₂O₃, we conclude that Cr₂Te₄O₁₁ might be the possible ternary compound in the final product. The final product was amorphous in nature. Hence HRTEM and XRD studies were not informative.

The product of reaction between Te NWs and KMnO₄ was also analyzed using Raman and XPS (Figure 9). As previously discussed, before the reaction, Te NWs showed three prominent features at 149 and 270 cm⁻¹ and a broad feature in the 380–480 cm⁻¹ window (marked with black dotted lines).^{29,34} Initial Te NWs showed three prominent features in the Raman spectrum at 149, 270, and 480 cm⁻¹ (marked with black lines). After the reaction, all oxygenated features became prominent. Additional features were seen at 392, 520, 630, and 712 cm⁻¹. Features at 392 and 712 cm⁻¹ are due to the bending and symmetric stretching modes of Te–O of TeO₂, indicating that the reaction product of Te NWs might be TeO₂ in this case as well.³⁴ The features at 520 and 630 cm⁻¹ can be assigned to the Mn–O stretching of MnO₂ (marked with yellow dotted lines).⁴¹

The oxidation states of the elements after reaction were analyzed using XPS (Figure 9 B₁–B₂). XPS measurements showed that Te (0) in Te NWs is converted to Te(IV). Te showed 3d_{3/2} and 3d_{5/2} centered at 576.4 and 586.6 eV, respectively, corresponding to Te(IV).³⁶ Concomitantly, Mn(VII) is converted to Mn(IV), pointing to the redox reaction between Te NWs and KMnO₄. XPS scan in the Mn 2p region showed two peaks at 641.7 and 653.3 eV corresponding to Mn 2p_{3/2} and Mn 2p_{1/2} (with a ΔJ of 11.6 eV), confirming the reduction product of KMnO₄ to be MnO₂.^{36,42,43} The Raman, XPS, and EDAX analysis indicate the formation of a ternary compound of Mn, Te, and O in this case as well. The possible ternary compounds in the Mn–Te–O system are: Mn₆Te₅O₁₆, MnTeO₃, Mn₂Te₃O₈, MnTe₂O₅, MnTe₆O₁₃, Mn₃TeO₆, and Mn₂TeO₆.⁴⁴ Raman and XPS data indicated that Te is existing as Te(IV) and Mn(IV). Raman features corresponding to TeO₂ and MnO₂ were seen in Raman spectrum. ΔJ values observed in XPS measurements also indicate the presence of TeO₂ and MnO₂. Mn₂TeO₆ is known to have a 2:1 MnO₂–TeO₂ phase and can give rise to observed Raman and XPS spectra.⁴⁴ The oxidation state of Te and Mn obtained from XPS also points to the Mn₂TeO₆ phase. Therefore, it was concluded that the final product formed is Mn₂TeO₆.

Mechanism of the Morphology Change. Scheme 1 summarizes the different stages of reaction between Te NWs and CrO₃/KMnO₄. Both reactions involve four steps, as depicted in the Scheme. The first step in both of the cases is the formation of

core–shell-like structures by the deposition of the reduction product. In the CrO_3 case, further reaction between Te and CrO_3 results in the formation of pits on the NWs. Formation of these pits happens more readily near the tips of the NWs. Specific formation of pits on the edge of the nanosystems is reported.^{23,45} Simultaneously, some worm-like structures also form. From EDAX analysis, it was concluded that these are reduction products of CrO_3 . Further redox reaction accompanied by NKE results in the formation of hollow structures (Scheme 1A). The worm-like structures progressively disappeared as the reaction progressed. In the case of reaction with KMnO_4 (Scheme B), after the formation of the shell, the NWs bundle up with a film forming around them. The film is due to the reduction products of KMnO_4 , as indicated by the EDAX measurement (Supporting Information, Figure S5). Subsequently, the NWs started to bend and became hollow (Figure 6D₃). Further reaction resulted in the formation of carbon onion-like structures. Redox reactions are reported to form hollow structures.¹⁹ Normally they are fast, and most of these will result in one-component structures. Recent studies show that even in these reactions NKE might be playing some role.⁴⁵ Oxide structures and to a large extent ternary oxides are known to form through the Kirkendall effect.^{46,47} Hence it was concluded that the redox reaction between Te NWs and $\text{CrO}_3/\text{KMnO}_4$ and the concomitant NKE is the reason for the observed morphology changes. However, the reason for the difference in structure of the end products is not well understood. The difference in reactivity of precursors used is reported to influence the shape of resulting structure.^{48,49} Moreover, it is reported that in NKE, depending on the rate of diffusion, either single or multiple voids can form.⁵⁰ When the diffusion through the interface toward the exterior is faster compared with that toward the interior, pits formed will collapse with each other. This results in the formation of structures with completely hollow interior, but when the diffusion outward is slower, multiple pits are formed and the diffusion rate is not enough to cause the voids to combine into a single void.⁵⁰ In the present case, diffusion of TeO_2 formed might be faster in the case of CrO_3 , resulting in the formation of a single void (hollow nanowires), and in the case of KMnO_4 , the diffusion might not be fast enough; as a result, multiple voids are formed (carbon onion-like structure). Hence, the difference in reactivity and rate of diffusion associated with the species involved (KMnO_4 and CrO_3) is believed to be the reason for the difference in the final structure, but more investigations are needed to establish the same.

Effect of pH on the Reaction. Redox reactions and NKE are known to be highly dependent on pH and temperature. The effects of pH and temperature on the reactions were investigated. Dependence of pH was checked first. Reduction of Cr(VI) is known to be highly pH-dependent.^{51–53} The reduction is reported to happen faster under acidic (<4), slower under near-neutral, and negligible under alkaline (≥ 10) pH conditions.^{51–53} The present reactions were done at three different pH values (3, 7, 10). The initial NWs were near neutral after two rounds of centrifugation redispersion cycles. The pH of Te NWs was adjusted by the addition of dil. HCl or dil. NaOH.

Figure 10A shows the reaction between Te NW and CrO_3 under acidic conditions (pH ~ 3). The NWs under initial conditions (pH ~ 6.5) took 14 days to complete the reaction (Figure 1C). At pH ~ 3 , the reaction was found to be much faster, and it was completed in 6 days (Figure 10A). However, at pH ~ 10 , the reaction was negligible. Even after 4 weeks, only minor changes were observed in UV/vis spectra, indicating negligible reaction under alkaline conditions (Figure 10B). At acidic pH,

the Cr(VI)/Cr(III) has a reduction potential of 1.38, whereas at alkaline pH it is -0.11 .^{52,53} Hence in acidic pH, the reaction becomes faster and in alkaline pH negligible reaction happens. Reaction of KMnO_4 and the reduction of Mn(VII) is also known to depend on pH.⁵⁴ Similar to the CrO_3 case, the reaction happened faster at acidic pH. The higher reduction potential of Mn(VII)/Mn(IV) in acidic pH ($+1.71$ V)^{52,53} might be the reason for the increased rate. Figure 10C shows the UV/vis spectra of the reaction between Te NWs and KMnO_4 at pH ~ 3 . For the initial NWs (pH ~ 6.5), the reaction was completed in 10 days, but at pH ~ 3 , the reaction was completed in 5 days. When the pH was adjusted to alkaline range (pH ~ 10), unlike in CrO_3 , reaction occurs in this case. The reduction potential for Mn(VII)/Mn(IV) couple in alkaline pH is $+0.60$ V,^{52,53} which is enough to oxidize Te to TeO_2 and hence resulted in the reaction, but for the completion of reaction, it took nearly 15 days. This was attributed to the lower reduction potential in the alkaline medium.

Effect of Temperature on the Reaction. The effect of temperature on the reaction was also checked. All reactions were done under ambient conditions at room temperature (30 ± 2 °C). Reactions were done at lower (10 °C) and higher (50 °C) temperatures as well. The increase in temperature increased the reaction rate in both the cases, whereas decrease in temperature resulted in decreased rate.^{28,55} In the case of CrO_3 , at 50 °C, the reaction was completed in 8 days (Figure 11A). The same reaction was not completed even after 28 days when it was done at 10 °C (Figure 11B). A similar trend was seen in the case of reaction with KMnO_4 as well. At 50 °C (Figure 11C), the reaction rate increased and the reaction was completed in 4 days, and at 10 °C, even after 20 days the reaction was not complete and a small hump indicated the residual Te NWs remained. This proves that the pH of the medium and the reaction temperature greatly influenced the reaction.

Effect of Concentration of $\text{CrO}_3/\text{KMnO}_4$. The effect of concentration on reaction was also looked into. The concentration of $\text{CrO}_3/\text{KMnO}_4$ added was varied to find out the optimum value. The original concentration used was 1 mM. When the concentration was decreased to 0.1 mM, the reaction was not completed even after 16 days of reaction in the case of CrO_3 . Peak II of Te NWs was seen even after 16 days of reaction, pointing to the incomplete reaction (Supporting Information, Figure S8A). The reaction was followed for 24 days but no further changes happened. When the concentration of CrO_3 was increased (10 mM), the NWs underwent aggregation and separated from the solution. Hence, reaction happened only to a limited extent. Therefore, the concentration required for the reaction was fixed at 1 mM. Similar observation was seen in the case of KMnO_4 as well. At lower concentration (0.1 mM, Supporting Information, Figure S8B), the reaction was not complete after 24 days. After 15 days, no appreciable reaction happened, and a prominent peak II was seen in all cases, pointing to incomplete reaction. Similar to the CrO_3 case, the NWs aggregated and separated from solution at higher concentration of KMnO_4 (10 mM); consequently, the reaction was minimal.

CONCLUSIONS

A room-temperature strategy to fabricate ternary oxide hollow nanostructures from Te NWs was devised by combining redox chemistry and NKE. Reactions of Te NWs with common oxidants such as CrO_3 and KMnO_4 were probed. The reaction resulted in a change in morphology of the NW. In the case of

CrO₃, the 1D structure of the nanowire remained intact, and the morphology changed to hollow NWs. Time-dependent TEM analysis showed that first a shell is formed around the NWs. Further reaction results in the formation of hollow structures. As the reaction goes on, crystallinity of the material decreased. The intermediate TEM showed the periphery of the material to be amorphous, whereas the inside portion, consisting of the reacted part of Te NWs, was found to be crystalline with clear lattice structure. After completion of the reaction, no lattice was seen. XPS as well as Raman spectroscopy showed a redox reaction between Te NWs and CrO₃ where Te(0) is oxidized to Te(IV) and Cr(VI) is reduced to Cr(III). From the EDAX, Raman, and XPS data, it was concluded that the final structure is composed of Cr₂Te₄O₁₁, a ternary compound of Te, Cr, and O. When the reaction happened with KMnO₄, the product showed a carbon onion-like structure. Time-dependent TEM analysis showed the different stages of the reaction. The morphology change was concluded to be due to a redox reaction between Te NWs and KMnO₄, which was proved by Raman as well as XPS measurements. The final structure is composed of a ternary compound of Mn, Te, and O, Mn₂TeO₆, which was proved by EDAX, Raman, and XPS analyses. The effects of temperature and pH on the reaction were examined, and it was found that acidic pH and increase in temperature are favorable for the reaction.

■ ASSOCIATED CONTENT

S Supporting Information. EDAX analysis of intermediate structures during the reaction between Te NWs and CrO₃/KMnO₃ and time-dependent UV/vis spectra of reaction with lower concentration of CrO₃/KMnO₄. This material is available free of charge via the Internet at <http://pubs.acs.org>.

■ AUTHOR INFORMATION

Corresponding Author

*E-mail: pradeep@iitm.ac.in. Fax: 91-44-2257-0545/0509.

■ ACKNOWLEDGMENT

We thank the Nanoscience and Nanotechnology Initiative of DST, Government of India, for supporting our research program.

■ REFERENCES

- (1) Zhang, J. Z. *Acc. Chem. Res.* **1997**, *30*, 423–429.
- (2) Tenne, R. *Angew. Chem., Int. Ed.* **2003**, *42*, 5124–5132.
- (3) Kijima, T.; Yoshimura, T.; Uota, M.; Ikeda, T.; Fujikawa, D.; Mouri, S.; Uoyama, S. *Angew. Chem., Int. Ed.* **2004**, *43*, 228–232.
- (4) Lee, W.; Scholz, R.; Nielsch, K.; Gösele, U. *Angew. Chem., Int. Ed.* **2005**, *44*, 6050–6054.
- (5) Mao, Y.; Banerjee, S.; Wong, S. S. *Chem. Commun.* **2003**, 408–409.
- (6) Jia, C.-J.; Sun, L.-D.; Yan, Z.-G.; Pang, Y.-C.; You, L.-P.; Yan, C.-H. *J. Phys. Chem. C* **2007**, *111*, 13022–13027.
- (7) Schmidt, O. G.; Eberl, K. *Nature* **2001**, *410*, 168–168.
- (8) Goldberger, J.; He, R.; Zhang, Y.; Lee, S.; Yan, H.; Choi, H.-J.; Yang, P. *Nature* **2003**, *422*, 599–602.
- (9) Steinhart, M.; Wendorff, J. H.; Greiner, A.; Wehrspohn, R. B.; Nielsch, K.; Schilling, J.; Choi, J.; Gosele, U. *Science* **2002**, *296*, 1997.
- (10) Mao, Y.; Park, T.-J.; Wong, S. S. *Chem. Commun.* **2005**, 5721–5735.
- (11) Li, Y.; Ma, X. L. *Phys. Status Solidi A* **2005**, *202*, 435–440.

- (12) Xianqin, W.; Jonathan, C. H.; Jose, A. R.; Carolina, B.; Marcos, F.-G. *J. Chem. Phys.* **2005**, *122*, 154711.
- (13) Jie, J.; Wang, G.; Han, X.; Fang, J.; Yu, Q.; Liao, Y.; Xu, B.; Wang, Q.; Hou, J. G. *J. Phys. Chem. B* **2004**, *108*, 8249–8253.
- (14) Leonard, S. R.; Snyder, B. S.; Brewer, L.; Stacy, A. M. *J. Solid State Chem.* **1991**, *92*, 39–50.
- (15) Pang, C.; Yan, B.; Liao, L.; Liu, B.; Zheng, Z.; Wu, T.; Sun, H.; Yu, T. *Nanotechnology* **2010**, *21*, 465706.
- (16) Calvo, C.; Ng, H. N.; Chamberland, B. L. *Inorg. Chem.* **1978**, *17*, 699–701.
- (17) Son, D. H.; Hughes, S. M.; Yin, Y.; Alivisatos, A. P. *Science* **2004**, *306*, 1009–1012.
- (18) Moon, G. D.; Ko, S.; Xia, Y.; Jeong, U. *ACS Nano* **2010**, *4*, 2307–2319.
- (19) Cogley, C. M.; Xia, Y. *Mater. Sci. Eng. R.* **2011**, *70*, 44–62.
- (20) Sreeprasad, T. S.; Samal, A. K.; Pradeep, T. *Bull. Mater. Sci.* **2008**, *31*, 219–224.
- (21) Sajanlal, P. R.; Sreeprasad, T. S.; Samal, A. K.; Pradeep, T. *Nano Rev.* **2011**, *2*, 5883.
- (22) Ng, M. T.; Boothroyd, C. B.; Vittal, J. J. *J. Am. Chem. Soc.* **2006**, *128*, 7118–7119.
- (23) Jiang, X.; Mayers, B.; Wang, Y.; Cattle, B.; Xia, Y. *Chem. Phys. Lett.* **2004**, *385*, 472–476.
- (24) Xia, Y.; Yang, P.; Sun, Y.; Wu, Y.; Mayer, B.; Gates, B.; Yin, Y.; Kim, F.; Yan, H. Q. *Adv. Mater.* **2003**, *15*, 353–389.
- (25) *Lange's Handbook of Chemistry*, 13th ed.; Dean, J. A., Ed.; McGraw-Hill: New York, 1985.
- (26) Zhang, B.; Hou, W. Y.; Ye, X. C.; Fu, S. Q.; Xie, Y. *Adv. Funct. Mater.* **2007**, *17*, 486–492.
- (27) Wang, Y.; Tang, Z.; Podsidlo, P.; Elkasabi, Y.; Lahann, J.; Kotov, N. A. *Adv. Mater.* **2006**, *18*, 518–522.
- (28) Sreeprasad, T. S.; Samal, A. K.; Pradeep, T. *J. Phys. Chem. C* **2009**, *113*, 1727–1737.
- (29) Sreeprasad, T. S.; Samal, A. K.; Pradeep, T. *Chem. Mater.* **2009**, *21*, 4527–4540.
- (30) Samal, A. K.; Pradeep, T. *J. Phys. Chem. C* **2009**, *113*, 13539–13544.
- (31) Samal, A. K.; Pradeep, T. *J. Phys. Chem. C* **2010**, *114*, 5871–5878.
- (32) Lin, Z.-H.; Yang, Z.; Chang, H.-T. *Cryst. Growth Des.* **2007**, *8*, 351–357.
- (33) Metz, W.; Meyer-Spasche, H. *Synth. Met.* **1979**, *1*, 63–75.
- (34) Qin, A.; Fang, Y.; Tao, P.; Zhang, J.; Su, C. *Inorg. Chem.* **2007**, *46*, 7403–7409.
- (35) Farrow, R. L.; Nagelberg, A. S. *Appl. Phys. Lett.* **1980**, *36*, 945–947.
- (36) Moulder, J. F.; Stickle, W. F.; Soble, P. E.; Bomben, K. D. *Handbook of X-Ray Photoelectron Spectroscopy*; Perkin-Elmer Corporation: Eden Prairie, MN, 1992.
- (37) Soundararajan, D.; Mangalaraj, D.; Nataraj, D.; Dorosinski, L.; Santoyo-Salazar, J.; Jeon, H. C.; Kang, T. W. *Appl. Surf. Sci.* **2009**, *255*, 7517–7523.
- (38) Grohmann, I.; Kemnitz, E.; Lippitz, A.; Unger, W. E. S. *Surf. Interface Anal.* **1995**, *23*, 887–891.
- (39) Bowden, F. L.; Heveltdt, P. F.; Watson, D. J.; Howell, J. A. S.; Wyeth, P.; Berry, F. J.; Evans, J.; Clack, D. W.; Davis, R.; McAuliffe, C. A.; Johns, D. M. *Inorganic Chemistry of the Transition Elements*; RSC Publishing: Cambridge, U.K., 1978; Vol. 6.
- (40) Meunier, G.; Frit, B.; Galy, J. *Acta Crystallogr., Sect. B* **1976**, *32*, 175–180.
- (41) Liang, S.; Teng, F.; Bulgan, G.; Zong, R.; Zhu, Y. *J. Phys. Chem. C* **2008**, *112*, 5307–5315.
- (42) Subramanian, V.; Zhu, H.; Wei, B. *Chem. Phys. Lett.* **2008**, *453*, 242–249.
- (43) Sreeprasad, T. S.; Maliyekkal, S. M.; Lisha, K. P.; Pradeep, T. *J. Hazard. Mater.* **2011**, *186*, 921–931.
- (44) Narasimhan, T. S. L.; Sai Baba, M.; Viswanathan, R. *J. Phys. Chem. B* **2002**, *106*, 6762–6770.

- (45) Fan, H. J.; Gösele, U.; Zacharias, M. *Small* **2007**, *3*, 1660–1671.
- (46) Yin, Y.; Rioux, R. M.; Erdonmez, C. K.; Hughes, S.; Somorjai, G. A.; Alivisatos, A. P. *Science* **2004**, *304*, 711–714.
- (47) Jin fan, H.; Knez, M.; Scholz, R.; Nielsch, K.; Pippel, E.; Hesse, D.; Zacharias, M.; Gosele, U. *Nat. Mater.* **2006**, *5*, 627–631.
- (48) Smith, D. K.; Luther, J. M.; Semonin, O. E.; Nozik, A. J.; Beard, M. C. *ACS Nano* **2011**, *5*, 183–190.
- (49) Zhong, H.; Lo, S. S.; Mirkovic, T.; Li, Y.; Ding, Y.; Li, Y.; Scholes, G. D. *ACS Nano* **2010**, *4*, 5253–5262.
- (50) Railsback, J. G.; Johnston-Peck, A. C.; Wang, J.; Tracy, J. B. *ACS Nano* **2010**, *4*, 1913–1920.
- (51) He, Y. T.; Traina, S. J. *Environ. Sci. Technol.* **2005**, *39*, 4499–4504.
- (52) Bard, A. J.; Parsons, R.; Jordan, J. *Standard Potentials in Aqueous Solutions*; Marcel Dekker: New York, 1985.
- (53) Greenwood, N. N.; Earnshaw, A. *Chemistry of the Elements*, 2nd ed.; Butterworth-Heinemann, Oxford, U.K., 1997.
- (54) Rifai, M. K.; Jamal, M. M. *J. Univ. Chem. Technol. Metall.* **2009**, *44*, 275–280.
- (55) Goshu, I.; Tsarev, Y.; Kostrov, V. *Russ. J. Appl. Chem.* **2007**, *80*, 2024–2027.